

# Designing minimal and scalable insect-inspired multi-locomotion millirobots

Zhenishbek Zhakypov<sup>1</sup>, Kazuaki Mori<sup>2</sup>, Koh Hosoda<sup>2</sup> & Jamie Paik<sup>1\*</sup>

**In ant colonies, collectivity enables division of labour and resources<sup>1–3</sup> with great scalability. Beyond their intricate social behaviours, individuals of the genus *Odontomachus*<sup>4</sup>, also known as trap-jaw ants, have developed remarkable multi-locomotion mechanisms to ‘escape-jump’ upwards when threatened, using the sudden snapping of their mandibles<sup>5</sup>, and to negotiate obstacles by leaping forwards using their legs<sup>6</sup>. Emulating such diverse insect biomechanics and studying collective behaviours in a variety of environments may lead to the development of multi-locomotion robotic collectives deployable in situations such as emergency relief, exploration and monitoring<sup>7</sup>; however, reproducing these abilities in small-scale robotic systems with simple design and scalability remains a key challenge. Existing robotic collectives<sup>8–12</sup> are confined to two-dimensional surfaces owing to limited locomotion, and individual multi-locomotion robots<sup>13–17</sup> are difficult to scale up to large groups owing to the increased complexity, size and cost of hardware designs, which hinder mass production. Here we demonstrate an autonomous multi-locomotion insect-scale robot (millirobot) inspired by trap-jaw ants that addresses the design and scalability challenges of small-scale terrestrial robots. The robot’s compact locomotion mechanism is constructed with minimal components and assembly steps, has tunable power requirements, and realizes five distinct gaits: vertical jumping for height, horizontal jumping for distance, somersault jumping to clear obstacles, walking on textured terrain and crawling on flat surfaces. The untethered, battery-powered millirobot can selectively switch gaits to traverse diverse terrain types, and groups of millirobots can operate collectively to manipulate objects and overcome obstacles. We constructed the ten-gram palm-sized prototype—the smallest and lightest self-contained multi-locomotion robot reported so far—by folding a quasi-two-dimensional metamaterial<sup>18</sup> sandwich formed of easily integrated mechanical, material and electronic layers, which will enable assembly-free mass-manufacturing of robots with high task efficiency, flexibility and disposability.**

The jaw jump and leg jump multi-locomotion mechanisms that have evolved in trap-jaw ants are vital for traversing obstacles that are orders of magnitude larger than their millimetre-sized bodies, avoiding predators and covering large areas in search of food<sup>19</sup> (Extended Data Fig. 1). Engineering the ability to negotiate diverse terrain types at the meso-scale with design scalability remains a major challenge for the hardware design of locomotion mechanisms<sup>20</sup>. Some locomotion strategies, like jumping, necessitate considerable mechanical power<sup>21</sup> to achieve high take-off velocity, whereas walking requires relatively low power, and combining them into a compact robotic body with a minimal but tunable actuation power mechanism suitable for mass manufacturing is difficult. Existing small-scale multi-locomotion robots<sup>13–17</sup> possess individual mechanisms for each locomotion gait, with the associated increase in the number of gear trains, joints and links, which makes manufacturing difficult, and some require external electromagnetic actuation<sup>22,23</sup>. Neither of these approaches offers a compact, scalable and autonomous multi-locomotion robot

platform with capabilities similar to those that exist in the natural world.

We report the development of a multi-locomotion origami millirobot called Tribot (Fig. 1a), that addresses the multi-terrain mobility and scalability challenges of small-scale robots using a single, but versatile, locomotion mechanism. Tribot is a three-legged robot with dimensions of 30 mm (width), 58 mm (length) and 58 mm (height) with a Y-shaped flexure hinge (Y-hinge) at the centre, which can open and instantly close its legs by selective activation of three linear spring-type shape-memory alloy (SMA) actuators that function as ‘muscles’. Similar to the mandibles of the trap-jaw ant, the Y-hinge forms the basis of the snap-through mechanism that enables Tribot to leap and clear obstacles (Fig. 1b). When the Y-hinge is opened on any of the three sides by a pair of extensor SMA spring actuators to an angle slightly above 180° and then compressed uniaxially by a flexor SMA spring actuator, it experiences instability and ‘snaps through’ to the side of the applied compressive force with a variable speed proportional to the applied force (Fig. 1c). If the snap occurs at the hinge bottom, Tribot leaps vertically upwards in a height jump, similar to a jaw jump; if the snap is at any of the two hinge sides, the robot leaps horizontally in a distance jump (a leg-jump motion), which is beneficial for striding across gaps. Tribot can also combine both movements in a somersault jump for clearing barrier obstacles (Fig. 1d). In this case, the bottom SMA spring actuator activates shortly before triggering the side spring actuator that snaps the mechanism, so the robot leaps both vertically and horizontally in the air, flipping before landing. To use the same mechanism to enable the robot to walk with periodic short steps over textured terrains, we developed a ‘flic-flac’ locomotion strategy (also known as a forward-flip or handspring) similar to that used by the Moroccan spider *Cebrennus rechenbergi*<sup>24</sup>. Here, the actuator activation sequence is the same as for the somersault jump, except that the compression of the trigger actuator occurs at a low power so that the robot slightly hops and flips onto the next two legs. This manoeuvre can be produced multiple times, beginning from any of the robot’s edges. To achieve transport with fine steps on flat terrain, we incorporated a crawling strategy similar to that used by inchworms. We used the continuous bending ability of the Y-hinge at three sides combined with stick-slip rubber pads attached to the latches on two sides of the robot’s legs, that grip and release the ground contact. We embedded two torsional-sheet SMA actuators<sup>25</sup> with micro-heater layers into the latch folds, which change the angle of latches to produce controllable crawling in both the backward and forward directions.

To achieve scalability of the millirobot for collective applications, we combine the automated printed circuit board (PCB) assembly process and the flexibility of smart composite microstructure design<sup>26</sup> to facilitate the integration of the mechanical, material and electronic layers of the robot. This is achieved by processing the layers in two dimensions, laminating them layer by layer and assembling them into three dimensions by folding<sup>27,28</sup> (Fig. 1e). The PCB layer serves as structural backing and for robot autonomy by embedding off-the-shelf electronic components (including a microcontroller, distance and communication sensors and rechargeable batteries), and a Kapton polyimide layer

<sup>1</sup>Reconfigurable Robotics Laboratory, Swiss Federal Institute of Technology Lausanne, Lausanne, Switzerland. <sup>2</sup>Adaptive Robotics Laboratory, Osaka University, Osaka, Japan.  
\*e-mail: jamie.paik@epfl.ch

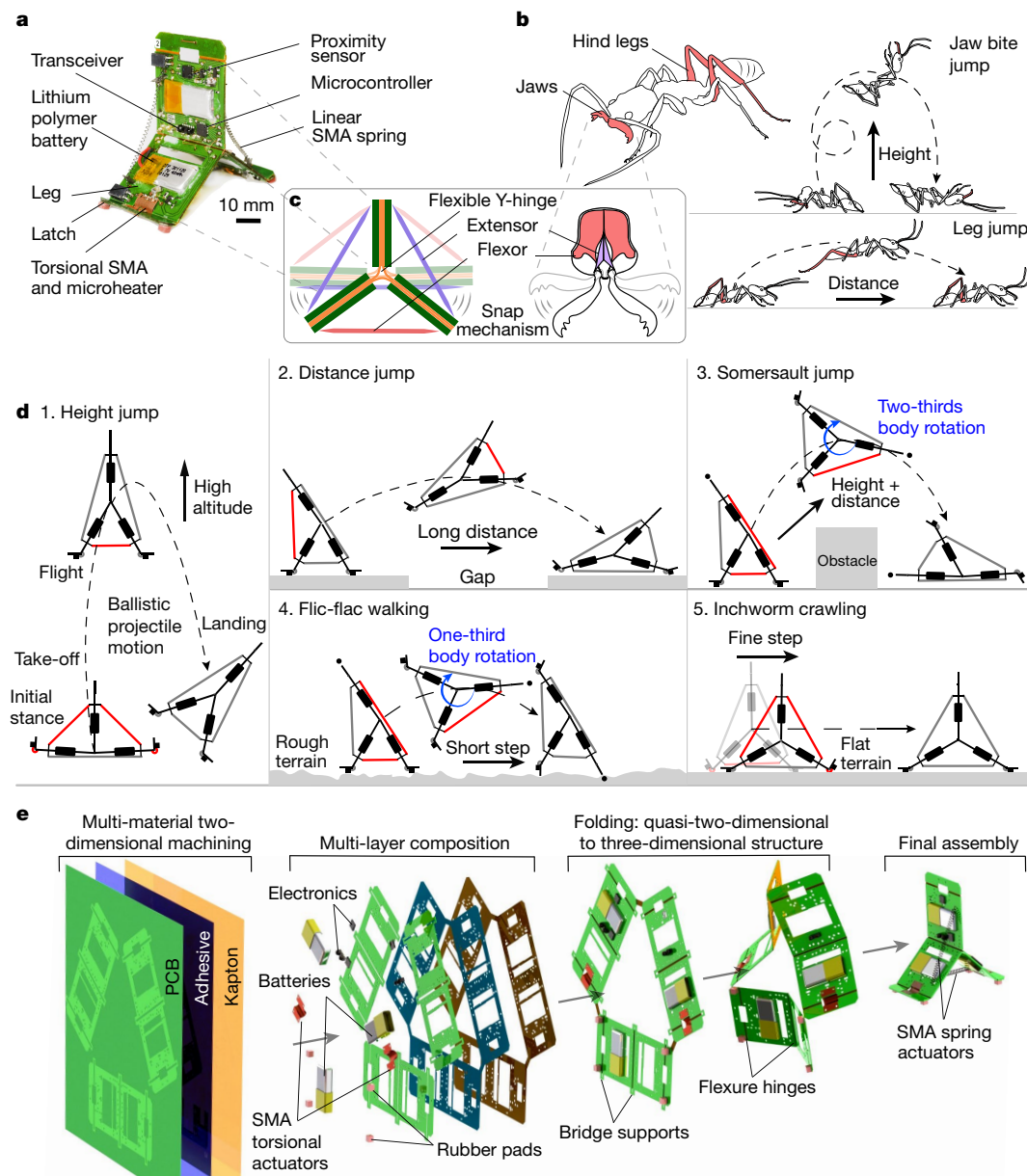


**Fig. 1 | Design and fabrication of the trap-jaw-ant-inspired Tribot multi-locomotion millirobot.** **a**, The untethered millirobot Tribot with a Y-hinge controlled by SMA actuators. **b**, The trap-jaw ant uses the snap of its mandible and its hind legs for jumping. **c**, The Y-hinge that connects the three legs ‘snaps through’ when compressed uniaxially with high force, and bends at low forces and angles less than  $180^\circ$ . **d**, Selective snapping

forms the flexure hinges. The integrated design of the actuators, mechanisms and surface-mounted electronics enables miniaturization of the robot; however, for the current version of Tribot, the major factor determining its size is the capacity of the off-the-shelf battery (3.7 V, 40 mA h), which occupies almost half of the robot’s PCB surface area and 40% of its body mass (Extended Data Table 1).

To validate the efficacy and repeatability of Tribot’s locomotion gaits, we conducted twelve original locomotion experiments: eleven independent gait tasks across the five gaits: height jumping, distance jumping, somersault jumping, walking and crawling, for various terrain, power and load conditions, each repeated six times, and one continuous ‘parkour’ (obstacle course) scenario employing multiple gaits, with smooth and rough terrain and an obstacle (Fig. 2, Extended Data Table 2). We studied the robot’s motion by recording each experiment on camera at a high frame rate of 250 frames per second (fps) for jumping and in real time (25 fps) for the walking and crawling

and bending of the Y-hinge generates five locomotion gaits: height (jaw) jumping, distance (leg) jumping, somersault jumping, flic-flac walking and inchworm crawling. The activation pattern is shown by the red-highlighted springs. **e**, The multilayer two-dimensional rapid fabrication and folding assembly process of Tribot.

gaits, and tracking the central Y-hinge using video analysis software. We assessed the robot’s vertical leaping capacity by studying height jumps on a flat surface, from its edges with and without the latches with rubber pads (Fig. 2a, Supplementary Video 1). For a trigger Joule heating power of 3.7 W to the flexor SMA spring actuator, Tribot jumps to a height of 140.6 mm on average (almost 2.5 times the robot’s height) from the edge without latches, owing to the minimal friction during take-off, and to a height of 72.5 mm from the edge with latches (Fig. 3a). We studied the robot’s horizontal distance jump for a trigger power of 3.7 W (Fig. 2b) and 2.7 W, and with an added payload of 5 g (more than 50% the robot’s body mass) at a trigger power of 3.7 W; the average jumping distance was 230 mm (almost four times its body length), 140 mm and 110 mm for these tests, respectively. The somersault jump gait was tested with a trigger power of 3.7 W; the average height and distance travelled were 88 mm and 100 mm, respectively, with an average two-thirds body rotation around its central axis in

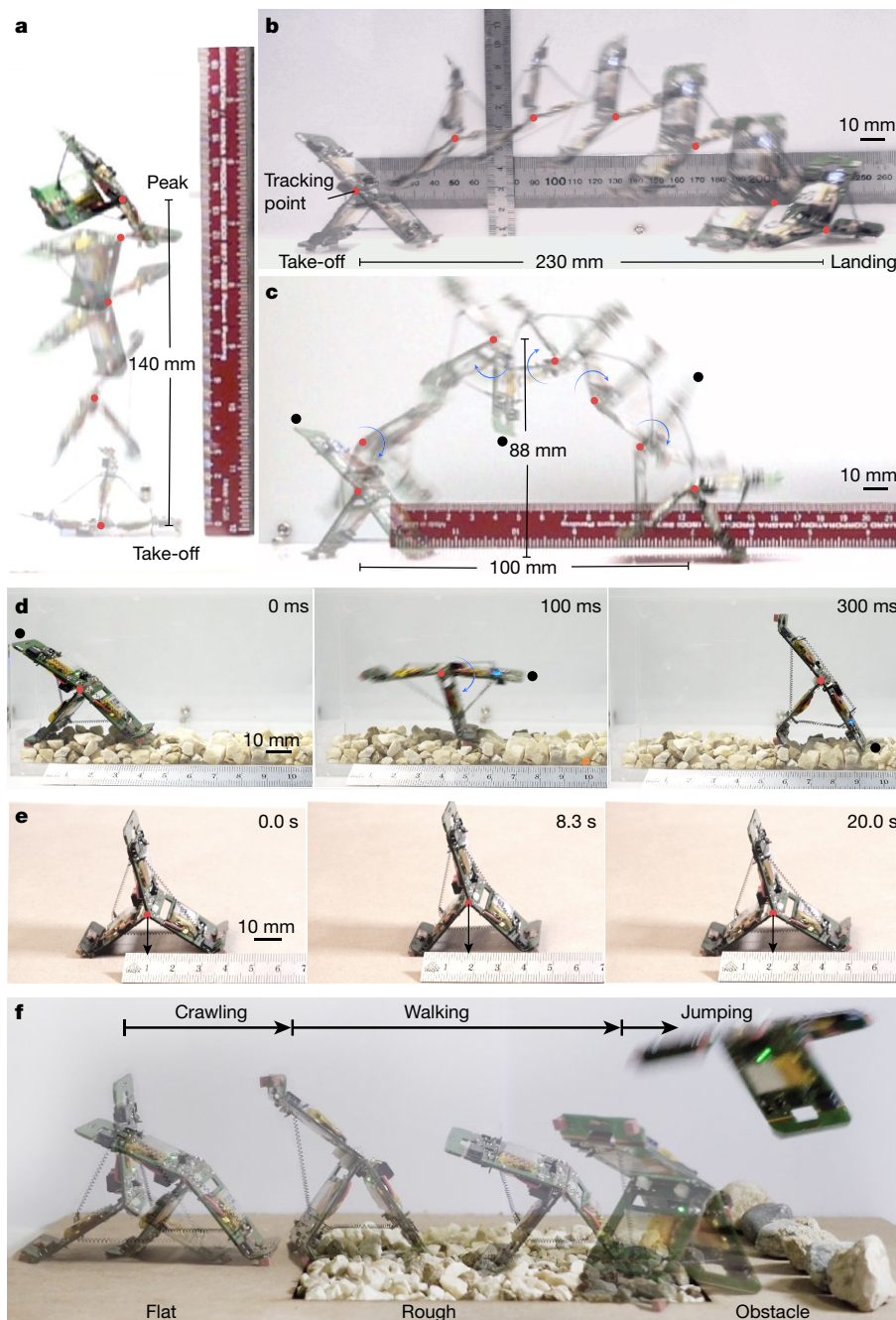


**Fig. 2 | Individual multi-locomotion experiments and their combination in the parkour scenario.** **a**, Tribot in height-jump gait on the non-latched side, from take-off to an average peak height of 140 mm. **b**, Tribot in distance-jump gait, from its initial stance to its landing position; 230 mm was the mean jump distance for a power input of 3.7 W. **c**, Tribot performing a somersault jump manoeuvre, during which it rotates in the air before landing; 88 mm was the mean jump height, and

100 mm the mean horizontal jump distance. **d**, Tribot performing a single flic-flac walking manoeuvre on rough terrain with raisin-sized stones.

**e**, The robot performing an inchworm crawling step using stick-slip motion on a smooth flat surface. **f**, Demonstration of the adaptability of Tribot's gait in a parkour setup comprising flat terrain, rough terrain and an obstacle. Tribot crawls through the flat section, walks on the rough terrain and somersaults over the obstacle.

the air. To test the effectiveness of the walking gait on flat and rough surfaces and of climbing up a flat slope of  $10^\circ$ , we instructed Tribot via remote control to perform three flic-flac manoeuvres on each terrain, such that it arrived back on its initial edge. To prevent the robot from deviating sideways, we placed it inside a transparent acrylic glass channel slightly wider than its body, with and without raisin-sized stones on the floor (Fig. 2d, Supplementary Video 2). Tribot completes an average repeatable step of 48.8 mm on the flat surface with a small 1.7 W trigger power, but the steps on the textured surface were not repeatable and considerably smaller, at 31.1 mm (Fig. 3b). This is probably due to minimal leg-ground contact with the textured surface, especially on the

edges without latches, which causes the legs to slip with each rotation. The average step on the slope was 28.8 mm and required about 30% more power to perform a full flip. We validated the robot's crawling locomotion on a flat surface and on a  $10^\circ$  slope (Fig. 2e, Supplementary Video 3). The robot was programmed to execute six consecutive crawling steps; the mean step size was 4.85 mm on the flat surface and just 2.61 mm on the slope, owing to slippage (Fig. 3c).

We assessed the generated mechanical power and energy cost of transport (COT) for all five gaits and compared Tribot's distance-jumping COT to those of existing small-scale multi-locomotion robots and insects (Fig. 3e, Extended Data Table 3). Tribot is the smallest and



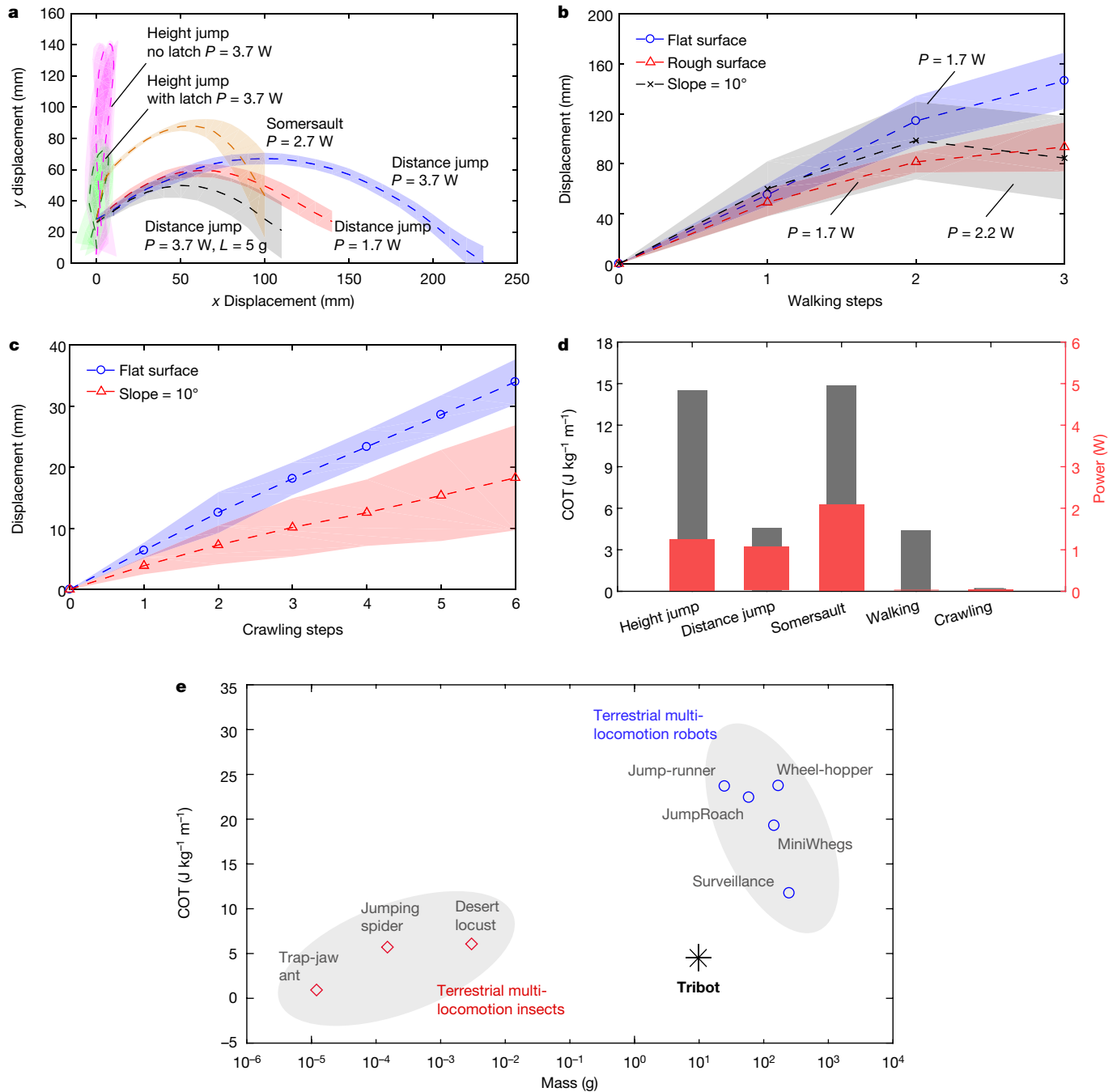


**Fig. 3 | Locomotion performance of Tribot in different conditions and its COT compared to robots and insects.**

**a**, Tribot’s motion projectiles for height, distance and somersault jumping for various SMA flexor spring Joule heating power inputs,  $P$ , and payloads,  $L$ , extracted from videos recorded at 250 fps. **b**, Tribot’s walking displacement per walking step on flat smooth terrain, flat rough terrain and a 10° smooth slope. The robot flips three times, returning to its initial orientation. **c**, Tribot’s inchworm

crawling displacement on a flat smooth surface and a smooth 10° slope, measured for six consecutive crawling step cycles. For **a–c**, the dashed lines and shaded regions indicate the mean and  $1\sigma$ , respectively, and each experiment is repeated six times. **d**, The mechanical power output and cost of transport for the five gaits. **e**, Tribot is smaller, lighter and has considerably lower COT for distance jumps than existing small-scale robots<sup>13–17</sup>; its characteristics are comparable to those of insects<sup>5,29,30</sup>.

lightest among the engineered systems surveyed and has substantially lower COT for distance jumps, comparable to that of trap-jaw ants<sup>5</sup>, the desert locust<sup>29</sup> and jumping spiders<sup>30</sup>.

To demonstrate Tribot’s multi-locomotion abilities on diverse terrain types and against an obstacle, we set up a parkour experiment (Fig. 2f). Owing to the difficulty in predicting the locomotion manoeuvre outcomes on rough terrain, we controlled the walking and jumping phases remotely, whereas the crawling locomotion was pre-programmed. In this test, Tribot crawled through the smooth section until it reached the rough terrain, where it switched to its walking gait. After four flips, Tribot arrived at the obstacle and jumped over it (Fig. 2f, Supplementary

Video 4). We observed discrepancy in the walking phase due to poor leg–ground contact that caused slippage, and the robot once landed on the wrong edge. However, because walking is possible on any edge, the robot was able to continue the manoeuvre, demonstrating its versatility.

To display task efficacy in a scalable collective of multi-locomotion millirobots, we set up two experiments, a division-of-labour scenario and a tandem-running scenario (Fig. 4, Supplementary Video 5), both executed autonomously. The first task was to move to a set position a prismatic object (a rectangular block) that was light enough for two robots to push but too heavy for one to move alone (Fig. 4a). Such a simple task, however, required five millirobots: two workers to push

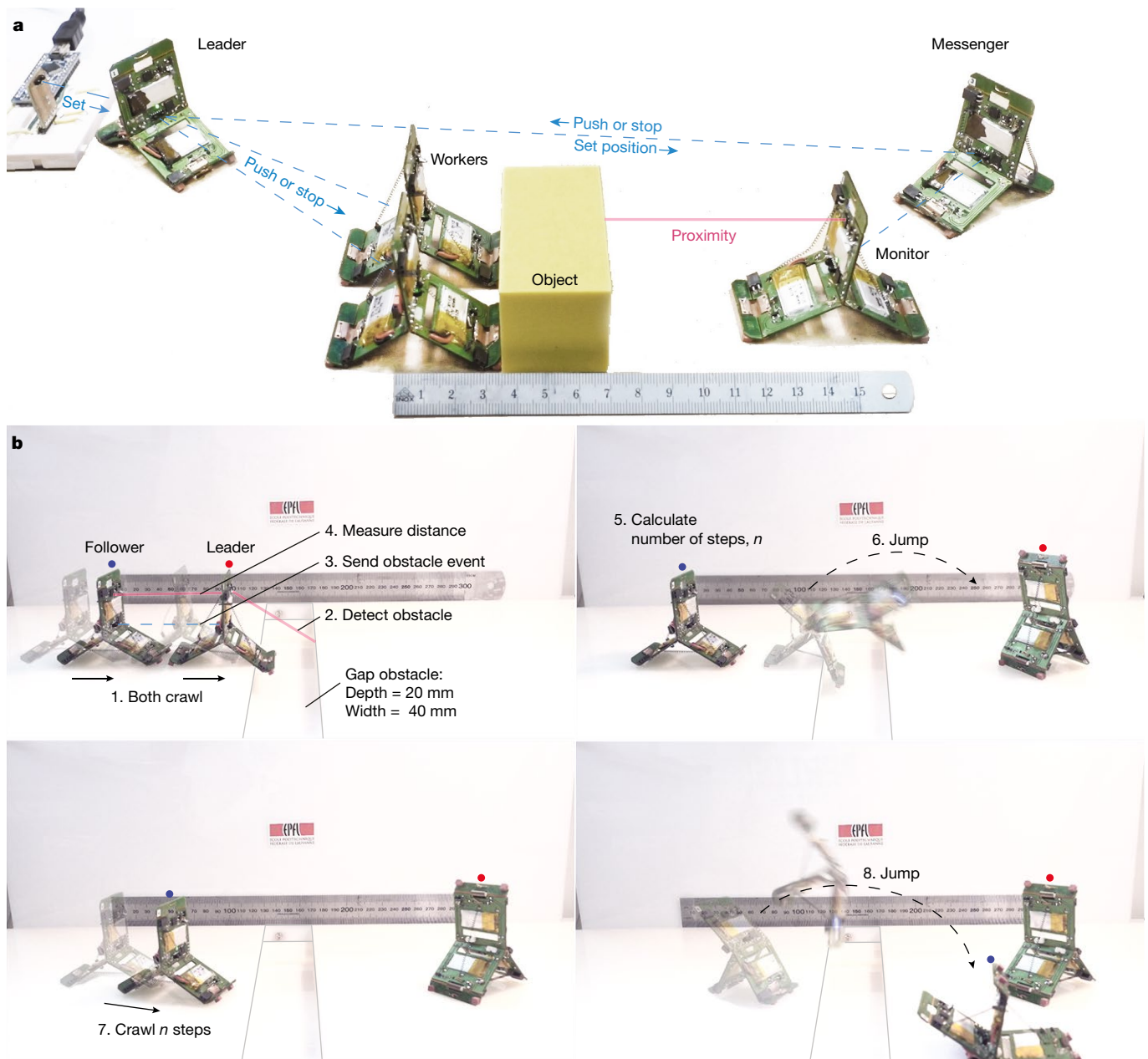


**Fig. 4 | Collective labour experiments.** **a**, Division-of-labour experiment. A rectangular prism was pushed to a desired position, using coordination between a leader, two workers, a monitor and a messenger robot. The leader orders two worker robots to push the object while the monitor measures the relative position of the object. As the object interrupts the two-way link between the leader and the monitor, the messenger maintains the communication link. **b**, Tandem-running experiment.

the object towards a monitor, who measured the relative closeness of the object using its proximity sensor and then informed the leader, who in turn coordinated the workers to continue or stop pushing. As the location of the prism interrupted the local communication between the leader and the monitor, the scheme required a messenger, who exchanged information between the leader and monitor via a path that avoided the prism. The data from the proximity sensor of the monitor robot show that the object travelled from a distance of 80 mm from the monitor robot to the programmed distance of 50 mm (Extended Data Fig. 3a). This experiment demonstrates the importance of millirobot scalability for effectively allocating tasks, manipulating objects and resolving communication issues with increased robot population.

Both robots crawl in a line (1) until the leader detects the gap obstacle (2) and transmits the information to the follower (3). Unlike the leader, the follower does not search for obstacles, and therefore saves energy. The follower measures the distance relative to the leader once (4) and calculates the total number of steps,  $n$ , to crawl to the obstacle (5), while the leader jumps over the obstacle (6). The worker crawls  $n$  steps (7) before safely jumping across the gap (8) (Supplementary Video 5).

To highlight the importance of robot multi-locomotion in collective tasks, we set up a tandem-running experiment with obstacle avoidance that fully demonstrates this functionality in Tribot. In the experiment, two robots, a leader and a follower (Fig. 4b), operate autonomously. The robots crawl in a line, with a fixed step size. The leader, while crawling, continuously scans for obstacles using its proximity sensor whereas the follower only checks messages from the leader, without energy expenditure for scanning. Both robots crawl until the leader detects an obstacle, upon which it conveys this information to the follower (Extended Data Fig. 3b). We chose a wide (40 mm) and deep (20 mm) gap as the obstacle, which may be crossed only by jumping. We demonstrate that the leader, when stopped at the gap edge and tilted forward, notifies the follower of the obstacle. Upon receiving the message, the

follower measures its distance relative to the leader only once and calculates the total number of steps to crawl by dividing that distance by the step size. Once the message is transmitted, the leader jumps over the gap, and the follower subsequently crawls and jumps, following its calculations, without falling in. This demonstration shows not only the expanded capabilities of multi-locomotion millirobot collectives, but also the benefits of collectivity in negotiating obstacles, such as allocating demanding tasks to a leader. Such millirobot tandem-running experiments can be used to further enhance the abilities of collectives of robots to navigate various terrain types and obstacles to effectively plan locomotion through teaching and learning.

We have presented an insect-scale origami robot with a minimal and scalable design that realizes multi-locomotion. The implementations that we present here are expected to facilitate future research into the effect of multi-locomotion ability on the collective behaviours, colony size and task distribution of social insects, that in turn will stimulate the development of algorithms for large-scale collectives of robots with expanded capabilities. The use of a customizable and mass-producible hardware platform forwards investigation into a variety of insect-inspired bio- and neuro-mechanics for millirobots. Although the current version of this hardware has limited manoeuvrability and sensing and computational capacity, it demonstrates applicability to real-world problems, such as emergency mitigation, environmental monitoring and exploration. We now aim to investigate comprehensive design methods<sup>28</sup> and automated fabrication processes to enable on-demand, 'push-button-manufactured' robots and mechanisms accessible to diverse research communities.

## Online content

Any methods, additional references, Nature Research reporting summaries, source data, extended data, supplementary information, acknowledgements, peer review information; details of author contributions and competing interests; and statements of data and code availability are available at <https://doi.org/10.1038/s41586-019-1388-8>.

Received: 31 August 2018; Accepted: 7 May 2019;

Published online 10 July 2019.

- Heyman, Y., Shental, N., Brandis, A., Hefetz, A. & Feinerman, O. Ants regulate colony spatial organization using multiple chemical road-signs. *Nat. Commun.* **8**, 15414 (2017).
- Gordon, D. M. The ecology of collective behavior. *PLoS Biol.* **12**, e1001805 (2014).
- Franks, N. R. & Richardson, T. Teaching in tandem-running ants. *Nature* **439**, 153 (2006).
- Sorger, D. M. & Zettel, H. On the ants (Hymenoptera: Formicidae) of the Philippine Islands: V. The genus *Odontomachus* Latreille, 1804. *Myrmecol. News* **14**, 141–163 (2011).
- Patek, S. N., Baio, J. E., Fisher, B. L. & Suarez, A. V. Multifunctionality and mechanical origins: ballistic jaw propulsion in trap-jaw ants. *Proc. Natl Acad. Sci. USA* **103**, 12787–12792 (2006).
- Sorger, D. M. Snap! Trap-jaw ants in Borneo also jump using their legs. *Front. Ecol. Environ.* **13**, 574–575 (2015).
- Fearing, R. S. Challenges for effective millirobots. In *IEEE Int. Sym. Micro-NanoMech. Hum. Sci.* 1–5 (IEEE, 2006).
- Rubenstein, M., Cornejo, A. & Nagpal, R. Programmable self-assembly in a thousand-robot swarm. *Science* **345**, 795–799 (2014).
- Kernbach, S. et al. Adaptive collective decision-making in limited robot swarms without communication. *Int. J. Robot. Res.* **32**, 35–55 (2013).
- Arvin, F., Murray, J., Zhang, C. & Yue, S. Colias: an autonomous micro robot for swarm robotic applications. *Int. J. Adv. Robot. Syst.* **11**, 113 (2014).
- Pickem, D. et al. The Robotarium: a remotely accessible swarm robotics research testbed. In *2017 IEEE Int. Conf. Rob. Autom.* 1699–1706 (IEEE, 2016).
- Weston-Dawkes, W. P., Ong, A. C., Majit, M. R. A., Joseph, F. & Tolley, M. T. Towards rapid mechanical customization of cm-scale self-folding agents. In *IEEE Int. Conf. Intel. Rob. Sys.* 4312–4318 (IEEE, 2017).
- Jung, G.P., Casarez, C. S., Jung, S. P., Fearing, R. S. & Cho, K. J. An integrated jumping–crawling robot using height-adjustable jumping module. In *2016 IEEE Int. Conf. Rob. Autom.* 4680–4685 (IEEE, 2016).
- Zhao, J., Yan, W., Xi, N., Mutka, M. W. & Xiao, L. A miniature 25 grams running and jumping robot. In *2014 IEEE Int. Conf. Rob. Autom.* 5115–5120 (IEEE, 2014).
- Morrey, J. M., Lambrecht, B., Horchler, A. D., Ritzmann, R. E. & Quinn, R. D. Highly mobile and robust small quadruped robots. In *2003 IEEE/RSJ Int. Conf. Intel. Rob. Sys.* **1**, 82–87 (IEEE, 2003).
- Song, G., Yin, K., Zhou, Y. & Cheng, X. A surveillance robot with hopping capabilities for home security. *IEEE Trans. Consum. Electron.* **55**, 2034–2039 (2009).
- Zhang, Y., Zhang, L., Wang, W., Li, Y. & Zhang, Q. Design and implementation of a two-wheel and hopping robot with a linkage mechanism. *IEEE Access* **6**, 42422–42430 (2018).
- Bertoldi, K., Vitelli, V., Christensen, J. & van Hecke, M. Flexible mechanical metamaterials. *Nat. Rev. Mater.* **2**, 17066 (2017).
- Larabee, F. J. & Suarez, A. V. Mandible-powered escape jumps in trap-jaw ants increase survival rates during predator–prey encounters. *PLoS One* **10**, e0124871 (2015).
- Bergbreiter, S. Effective and efficient locomotion for millimeter-sized microrobots. In *2008 IEEE/RSJ Int. Conf. Intel. Rob. Sys.* 4030–4035 (IEEE, 2008).
- Haldane, D. W., Plecnik, M. M., Yim, J. K. & Fearing, R. S. Robotic vertical jumping agility via series-elastic power modulation. *Sci. Rob.* **1**, eaag2048 (2016).
- Hu, W., Lum, G. Z., Mastrangeli, M. & Sitti, M. Small-scale soft-bodied robot with multimodal locomotion. *Nature* **554**, 81–85 (2018).
- Kim, Y., Yuk, H., Zhao, R., Chester, S. A. & Zhao, X. Printing ferromagnetic domains for untethered fast-transforming soft materials. *Nature* **558**, 274–279 (2018).
- Jäger, P. *Cebrennus* Simon, 1880 (Araneae: Sparassidae): a revisionary up-date with the description of four new species and an updated identification key for all species. *Zootaxa* **3790**, 319–356 (2014).
- Zhakypov, Z., Huang, J. L. & Paik, J. A novel torsional shape-memory alloy actuator: modeling, characterization, and control. *IEEE Robot. Autom. Mag.* **23**, 65–74 (2016).
- Wood, R.J., Avadhanula, S., Sahai, R., Steltz, E. & Fearing, R. S. Microrobot design using fiber-reinforced composites. *J. Mech. Des.* **130**, 052304 (2008).
- Zhakypov, Z. & Paik, J. Design methodology for constructing multi-material origami robots and machines. *IEEE Trans. Rob.* **34**, 151–165 (2018).
- Felton, S., Tolley, M., Demaine, E., Rus, D. & Wood, R. J. A method for building self-folding machines. *Science* **345**, 644–646 (2014).
- Bennet-Clark, H. C. The energetics of the jump of the locust *Schistocerca gregaria*. *J. Exp. Biol.* **63**, 53–83 (1975).
- Nabawy, M. R., Sivalingam, G., Garwood, R. J., Crowther, W. J. & Sellers, W. I. Energy and time optimal trajectories in exploratory jumps of the spider *Phidippus regius*. *Sci. Rep.* **8**, 7142 (2018).

**Acknowledgements** We thank H. Aonuma from the Complex Systems Research Group of Hokkaido University for providing insight into the behaviours of the trap-jaw ant. K.M. acknowledges financial support from the Japan Public–Private Partnership Student Study Abroad Program. This work is supported by the Swiss National Science Foundation (SNSF) ‘START’ Project and the Swiss National Center of Competence in Research (NCCR) Robotics.

**Reviewer information** Nature thanks Adam Stokes and the other anonymous reviewer(s) for their contribution to the peer review of this work.

**Author contributions** Z.Z., K.M., K.H. and J.P. designed the study and interpreted the results. Z.Z. and J.P. conceived the idea of developing multi-locomotion millirobot collectives. Z.Z. and K.M. developed the millirobot hardware platform. Z.Z. designed the multi-locomotion mechanisms and models, and K.M. designed the electronics and communication. Z.Z. produced the figures and videos. Z.Z. and J.P. wrote the manuscript with input from all authors.

**Competing interests** The authors declare no competing interests.

## Additional information

**Extended data** is available for this paper at <https://doi.org/10.1038/s41586-019-1388-8>.

**Supplementary information** is available for this paper at <https://doi.org/10.1038/s41586-019-1388-8>.

**Reprints and permissions information** is available at <http://www.nature.com/reprints>.

**Correspondence and requests for materials** should be addressed to J.P. **Publisher's note:** Springer Nature remains neutral with regard to jurisdictional claims in published maps and institutional affiliations.

© The Author(s), under exclusive licence to Springer Nature Limited 2019



## METHODS

**Design of robot locomotion mechanisms.** The snap-through and bending properties of the central flexible Y-hinge and the appropriate arrangement of the robot legs and latches by selective activation of the SMA actuators generate the height, distance and somersault jumping, walking or crawling gaits (Fig. 1d). These can be programmed on the onboard microcontroller or controlled remotely via a keyboard on a portable computer by setting the actuator activation sequence, duration and power through a custom graphical user interface. For height, distance and somersault jumping and for walking, the activation pattern (shown in Fig. 1d by the red-highlighted springs) transits the robot from an initial rest state to its stance and then to its take-off phases, but there are no presets for the flight and landing phases. The robot follows a ballistic projectile motion for all four manoeuvres after take-off, with different launch angle, velocity and body rotation during flight. We model the Y-hinge as a pin joint connecting three independently rotating legs (Extended Data Fig. 2). For distance jumping, somersault jumping and walking, the snap-through motion at the Y-hinge side closes two side legs, pushing the third rear leg against the ground at an angle  $\alpha$ , and the ground reaction force lifts the robot in the air. For height jumping, the snap-through of the Y-hinge bottom rapidly closes the two bottom legs against the ground, which in turn produce a ground reaction force that launches the robot vertically upwards. The kinematics of the robot flight between take-off and landing (first touchdown) in  $x$ - $y$  Cartesian coordinates are governed by a ballistic projectile motion given by

$$y = y_0 + x \tan \alpha - \frac{gx^2}{2v_0^2 \cos^2 \alpha} \quad (1)$$

where  $y_0$  is the initial height of the robot, measured between the centre of the Y-hinge and the ground at the instant of take-off,  $\alpha$  and  $v_0$  are the launch angle and velocity, respectively, and  $g$  is the gravitational acceleration. Because of the high uncertainty in predicting the surface area of the robot for each gait, especially owing to free-body rotation during somersault jumping and walking, we omit air-drag effects. The maximum horizontal travel distance,  $d$ , and vertical height,  $h$ , are then calculated by

$$h = \frac{v_0^2 \sin^2 \alpha}{2g}, \quad d = \frac{v_0^2 \sin 2\alpha}{g} \quad (2)$$

The jumping displacement of the robot is maximized by increasing  $v_0$  and attaining  $\alpha = \pi/2$  for height jumps and  $\alpha = \pi/4$  for distance and somersault jumping and walking. Although Tribot does not rotate considerably when performing height and distance jumps (at least during ascent), it performs, on average, a two-thirds body rotation for somersault jumping and a one-third body rotation for walking.

For crawling locomotion, the robot is in contact with the ground on its latched edges; the activation sequence using the linear and torsional actuators produces a periodic stick-slip motion (Fig. 1d, Extended Data Fig. 2c). In this sequence, the SMA torsional actuators raise the rubber pads to slip and drop them to stick, varying the contact friction. The crawling step is then calculated by

$$C = 4l(\sin \theta_o - \sin \theta_c) \quad (3)$$

where  $C$  is the crawling step size for a single stick-slip manoeuvre,  $l$  is the half-length of the leg, and  $\theta_o$  and  $\theta_c$  are the opening and closing angles between the bottom two legs (2 and 3), respectively, with  $\theta_o = \theta_c + \theta_2$  and  $\theta_2 = \theta_3$ .

To establish a generalized robot multi-locomotion dynamic model and to determine its velocity for each gait, we adopt a Euler–Lagrange method. Employing a Newtonian ( $F = ma$ ) approach is difficult for modelling not only multi-locomotion and multi-degree-of-freedom mechanisms, but also single-locomotion mechanisms. The energy-based approach of the Euler–Lagrange method provides insight into the locomotion mechanism performance in terms of stored energy and produced motion, and therefore enables design optimization of the system components that are responsible for motion. The total kinetic ( $E_K$ ) and potential ( $E_P$ ) energies of the robot are given by

$$E_K = \frac{1}{2} \sum_{i=1}^3 m_i v_i^2 + \frac{1}{2} \sum_{i=1}^3 J_i \omega_i^2 \quad (4)$$

$$E_P = \sum_{i=1}^3 m_i g h_i + \frac{1}{2} \sum_{i=1}^3 k_i s_i^2 \quad (5)$$

where  $m_i$ ,  $J_i$ ,  $v_i$ ,  $\omega_i$  and  $h_i$  are the mass, moment of inertia, Cartesian and angular velocities and height of the  $i$ th link (leg), respectively (Extended Data Fig. 2).  $k_i$  and  $s_i$  are the stiffness coefficient and the deflection of the  $i$ th SMA spring actuator, respectively. The Lagrangian function is then  $L = E_K - E_P$ . Because the high-speed (snap-through) rotation of links 1 and 2 and the low-speed (bending) rotation

of links 2 and 3 produce all five gaits, the equations of motion,  $\ddot{\theta} = \begin{bmatrix} \ddot{\theta}_1 \\ \ddot{\theta}_{i+1} \end{bmatrix}$ , where  $i = 1$  for the jumping and walking gaits and  $i = 2$  for crawling, can be computed by solving

$$\frac{d}{dt} \left( \frac{\partial \mathcal{L}}{\partial \dot{\theta}} \right) - \frac{\partial \mathcal{L}}{\partial \theta} = 0 \quad (6)$$

The masses and moments of inertia in equations (4), (5) for all three links are equal and constant, and so it is the spring actuator stiffness coefficients  $k_i$  that define the stored energy and thus determine the velocity of the links when they are released at the moment of snap-through. For our robot, the stiffness balance is set as  $k_1 + k_2 > k_3$  followed by  $k_3 > k_1 + k_2$  to generate the snap-through for the jumping and walking gaits, and  $k_1 > k_2 + k_3$  followed by  $k_2 + k_3 > k_1$  for crawling (Extended Data Fig. 2). The parameters of the actuators are tailored at design, but are also controllable during operation by changing the input Joule heating power, which varies the martensitic and austenitic temperature of the SMA, and hence also the stiffness<sup>27</sup> (see section ‘Actuation design’).

As the structure of Tribot necessitates a different configuration and orientation for each locomotion, we define a local coordinate frame ( $x'$ - $y'$ ) and global coordinate frame ( $x$ - $y$ ), which are related through a  $2 \times 2$  rotation matrix and the angle  $\alpha$  (Extended Data Fig. 2). As the position of the robot's centre of mass varies substantially between the stance and take-off states, we fix the origins for both coordinate systems at the centre of the Y-hinge. Then, the positions ( $p_i$ ) translational velocities ( $v_i$ ) and acceleration of links 1 and 2 are calculated by

$$p_i = \begin{bmatrix} x_i \\ y_i \end{bmatrix} = \begin{bmatrix} l(\sin(\theta_i + \alpha) - \sin \alpha) \\ -l(\cos(\theta_i + \alpha) - \cos \alpha) \end{bmatrix}, \quad i = 1, 2 \quad (7)$$

$$v_i = \sqrt{\dot{x}_i^2 + \dot{y}_i^2} = l\dot{\theta}_i, \quad i = 1, 2 \quad (8)$$

$$a_i = l\ddot{\theta}_i, \quad i = 1, 2 \quad (9)$$

where  $\dot{\theta}_i$  and  $\ddot{\theta}_i$  are equivalent to angular velocity  $\omega_i$  and acceleration  $\dot{\omega}_i$ , respectively. For height and distance jumping,  $\theta_1 \approx \theta_2$ , and for somersault jumping and walking,  $\theta_1 > \theta_2$ , owing to the brief activation of the bottom spring actuator before the snap-through, which limits the angular rotation of link 2. The overall robot velocity is then a sum of individual link velocities

$$m_T v = \sum_{i=1}^2 m_i v_i \quad (10)$$

Here,  $m_T$  and  $v = v_0$  are the mass and velocity of Tribot. The total actuation power  $P$  required to accelerate Tribot to a distance  $\Delta p$  between the stance and take-off can be calculated using

$$P = \frac{E_K}{\Delta p} v = \frac{m_T v^3}{2 \Delta p} \quad (11)$$

where  $E_K$  is the robot's kinetic energy. We can also calculate the COT for each locomotion by

$$\text{COT} = \frac{E_K}{m_T r} = \frac{v^2}{2r} \quad (12)$$

COT is measured in  $\text{J kg}^{-1} \text{m}^{-1}$  and  $r$  is the total travel distance between take-off and landing positions, corresponding to  $h$  for the height jump, to  $d$  for distance jumping, somersaulting and walking, and to the step size  $C$  for crawling locomotion. Tribot can jump a horizontal distance of 230 mm on average with a take-off velocity of  $1.44 \text{ m s}^{-1}$ , resulting in a low COT.

**Actuation design.** The previously mentioned locomotion mechanisms are produced by compressing and storing energy in the three SMA spring actuators that are Joule heated by passing a direct current, and in the two SMA torsional sheet actuators, motion is activated by the thermal conduction of the heat that is generated by the micro-heaters. To enable both fully automatic and remotely controlled activation of the actuators, with tunable power, we use a pulse-width-modulation method. We adjust the average electrical power  $P_{\text{avg}}$  to each actuator by controlling the switching duty cycle,  $0 \leq \text{duty} \leq 1$ , of five metal-oxide-semiconductor field-effect transistors in the software as  $P_{\text{avg}} = \text{duty} \times P_s$ . The supply power  $P_s$  is governed by Kirchhoff's rule so that  $P_s = \frac{V_s^2}{R_{\text{SMA}}}$ , where  $V_s$  is the battery supply voltage and  $R_{\text{SMA}}$  is the electrical resistance of either the SMA spring or the copper micro-heater layer of the SMA torsional sheet. In reality, the electrical resistance of the SMA slightly increases with temperature; however, for the plots in Fig. 3a, we fix it to  $2.2 \, \Omega$ , which is measured at room temperature (that is, when it is

martensite). Also, the SMA actuators stiffen proportionally to the applied heat between the martensitic (colder) and austenitic (hotter) temperatures. For the spring actuators, shear stress dominates owing to coil twisting, and its force-to-deflection relation for the martensitic and austenitic phases can be approximated by a linear relation without considering the detwinning effect

$$F = \frac{G(T)q^4}{8D^3N}\delta \quad (13)$$

Here,  $G(T)q^4/(8D^3N) = k$  is the SMA spring stiffness coefficient,  $\delta = \frac{\pi ND}{\cos\varphi_1}(\sin\varphi_f - \sin\varphi_i)$  is the spring deflection,  $q$  is the diameter of the wire,  $D$  is the coil diameter,  $N$  is the number of turns,  $\varphi_i$  and  $\varphi_f$  are the coil initial (compressed) and final (extended) pitch angles, and the shear modulus  $G$  is a function of the temperature  $T$  and varies between the martensitic minimum,  $G_M$ , and the austenitic maximum,  $G_A$ . The compression force increases substantially with increasing  $q$ ; however, higher currents are then required to heat the wire owing to the reduced resistance. This is an important trade-off in designing the actuators to generate sufficient force at low power for untethered applications. To ensure that Tribot can operate without an external power supply, we designed the spring actuators with  $q = 0.25$  mm,  $D = 0.9$  mm,  $N = 32$  or 33,  $G_A \approx 18$  GPa and  $G_M \approx 7$  GPa.

Unlike the linear spring actuator, the torsional actuator generates a bending moment; therefore, normal stress dominates its behaviour. Assuming pure bending of a thin sheet, the torque-to-angular-deflection relation can be approximated by

$$\tau = \frac{Y(T)I}{u}\theta \quad (14)$$

Here,  $\tau$  is the torque,  $Y$  is the temperature-dependent elastic modulus, which is in the range  $Y_M \leq Y \leq Y_A$  (between the martensitic and austenitic elastic moduli),  $I = \frac{wt^3}{12}$  is the second moment of inertia of a rectangular sheet with cross section  $w \times t$ ,  $u$  is the length of the curved section of the actuator and  $\theta$  is the sheet bending angle. For our torsional actuators<sup>24</sup>,  $t = 0.1$  mm,  $w = 8$  mm,  $u = 6.5$  mm,  $Y_A \approx 34$  GPa and  $Y_M \approx 19$  GPa. The external heater layer has a resistance of  $7 \Omega$ , is thin ( $<0.05$  mm) and consumes power as low as 0.5 W.

**Experimental design.** To measure the robot's height-, distance- and somersault-jumping trajectories and its walking and crawling steps, we set up eleven different experimental scenarios (Fig. 2, Extended Data Table 2). Each locomotion experiment is video-recorded and analysed using an open-source scientific video-tracking software called Tracker (<https://physlets.org/tracker/>). As the robot's leg snap-through motion occurs within 100 ms, we used a high-frame-rate camera (Sony Cyber-shot DSC-RX100 IV) with a recording speed of 250 fps to capture the robot's displacement in the  $x$ - $y$  plane. The camera was configured to a real-time (25 fps) recording speed for the walking, crawling and multi-locomotion parkour experiments. We used a ruler (SI units) to calibrate the captured videos in the  $x$  or  $y$  axis, which were then analysed in Tracker. For all locomotion manoeuvres, we tracked the robot's central  $Y$ -hinge in  $x$ - $y$  Cartesian coordinates from the instant of take-off to the instant of landing (first touchdown). We performed eleven independent experiments among all five gaits, each repeated six times. At the start of each run, Tribot was brought to an initial stance position. As each experiment measures twelve datasets (six each of  $x$  and  $y$  positions), with the data points not aligned in either of the axes, we interpolated each dataset using the Matlab *pchip* shape-preserving piecewise cubic interpolator function to align them in the  $x$  coordinate and then compute the mean for each experiment. We also calculated the average standard deviations in the  $y$  axis by taking the square root of the mean of variances (Extended Data Table 2). The standard deviation is plotted as a shaded region in each of the locomotion plots (Fig. 3a–c), using the Matlab *fill* function.

In the height-jump experiments (Figs. 2a, 3a), the robot is tested on two different edges: the sides with latches in contact with the ground and two sides with no latches (Supplementary Fig. 1b, Supplementary Video 1). The robot is controlled remotely for both experiments using a keyboard with a pre-set actuator activation power, displayed on a custom graphical user interface. For the loaded distance-jump experiment, we mounted a 5-g M8 stainless steel hexagonal nut at the robot's rear leg (Supplementary Video 1). To evaluate the robot's walking step size (Figs. 2d, 3b), we placed it into a 32-mm-wide channel made of transparent acrylic material to confine its lateral deviation while it flipped (Supplementary Video 2). For testing on a rough surface, we filled the channel floor with raisin-sized grains (FEPA F4 standard grain); they were removed for the smooth surface test. To evaluate the robot walking on a slope, we placed the channel on a smooth, inclined medium-density fibreboard with a slope of  $10^\circ$ .

To test the efficacy of the robot's crawling gait on different surfaces and on a slope, we programmed the robot to crawl with multiple steps on its edge with latches (Figs. 2e, 3c). We tested three terrain conditions: on sandpaper with roughness P100 (FEPA standard) and on medium-density fibreboard with a smooth finish, positioned horizontally (slope =  $0^\circ$ ) and then inclined to  $10^\circ$ . Tribot crawls by periodically applying friction on the ground surface with rubber pads and

sliding with the contact surface of the SMA torsional sheet actuator exposed after movement of the latch above the ground (a stick-slip movement), and so the surface interaction is essential in defining the crawling performance. We did not observe any horizontal propagation in the sandpaper test, owing to the increased friction between the torsional sheet actuator surface and the sandpaper, but the robot could crawl on the fibreboard with repeatable steps and even could crawl up a slope—although owing to sliding, it crawled with smaller steps on the slope than on a flat surface.

We computed the COT for each of Tribot's locomotion gaits (equation (12), Extended Data Table 3) and compared the distance-jumping COT to that of other multi-locomotion robots and insects, using take-off velocity, travel distance and mass data reported in the literature or extrapolated using equation (2). This comparison allowed effective benchmarking of engineered and biological systems in terms of locomotion efficiency and performance.

**Robot fabrication.** Robot hardware design for mass production should ideally be low-cost and customizable, for example using PCBs, which can be used to assemble diverse layouts of electronic components with versatile functionality in a matter of seconds. However, unlike PCBs, the mechanical design of several custom mechanisms and structural components dominates conventional robot construction, requiring meticulous assembly. Tribot's fabrication process allows robot multiplicity with minimal assembly effort (Fig. 1f). The robot's structure consists of two layers: a 300- $\mu$ m-thick double-sided FR-4 PCB for structural backing and electronics and a 50- $\mu$ m-thick Kapton polyimide film (DuPont) for the hinges, a material that is flexible and durable. The PCB workshop of the Swiss Federal Institute of Technology Lausanne mass-produced the PCB layer and the Kapton was cut on a laser micro-machining station (LAB 3550, Inno6). The two layers were bonded together using an adhesive film (Poli-Melt 701, Poli-Tape) and heat-pressed (Carver 3853CE, Carver) for 2 min at  $160^\circ\text{C}$  with 90 N pressure. Then, to attach the electronic components, we applied a solder paste (SMD291AX, Chip Quick) onto the 100- $\mu$ m-thick Kapton stencil placed on top of the PCB using a spatula, filling the component footprints. The stencil was gently removed, and the surface-mounted device components—including two infrared proximity sensors (VCNL4010, Vishay), two infrared transceivers (TFBS4711-TT1, Vishay) for communication, a microcontroller (ATTINY4313-MU, Atmel) and connectors and switches, among 50 other electronic components—were manually pick-placed onto the footprints. We then placed the PCB sheet for 3 min on a hot plate at  $200^\circ\text{C}$  for solder reflow. Then, three 3.7 V, 40 mA h rechargeable lithium ion polymer batteries (DTP301120, Datapower) were soldered onto the terminals, and the two SMA torsional actuators with attached micro-heaters, plus four 3-mm rectangular pads moulded from silicone rubber (Elastocil M4601, Wacker Chemie AG), were glued onto the two latches. After cutting off the support bridges across the PCB hinge gaps (Fig. 1f), the multilayer sheet was folded to pop up into the robot's three-legged three-dimensional structure. Finally, we soldered a few wires to electrically connect one leg to the other, install the SMA spring actuators and test the assembled robot.

Our design uses off-the-shelf components and the total cost of each robot is under US\$60. It takes approximately three hours for one skilled person to fabricate and manually assemble a robot. However, we could substantially reduce this time using an automated mass-production PCB assembly process. Our method facilitates processing of a wide range of materials with extremely fine features and greatly reduces the assembly effort, enabling low-cost and on-demand mass manufacturing of millirobots.

**Communication range.** Communication sensors allow multiple Tribot units to exchange information, interact and cooperate to execute collective tasks. Determining the sensor range helps to define the orientation and position of the next unit for a sustainable two-way (transmit–receive) communication link. The two infrared transceivers placed on either side of the robot's upper leg (the leg with no latch) produce a communication range of two symmetric sectors with a  $60^\circ$  angular opening, up to the maximum range of 1 m. For two robots to establish a two-way communication link, the maximum separation between them should not exceed 1 m and they should both be within the sector with orientation that meets the conditions

$$\beta_1 - \frac{\pi}{6} + n\pi \leq \gamma \leq \beta_1 + \frac{\pi}{6} + n, \quad n = \dots -1, 0, 1, \dots \quad (15)$$

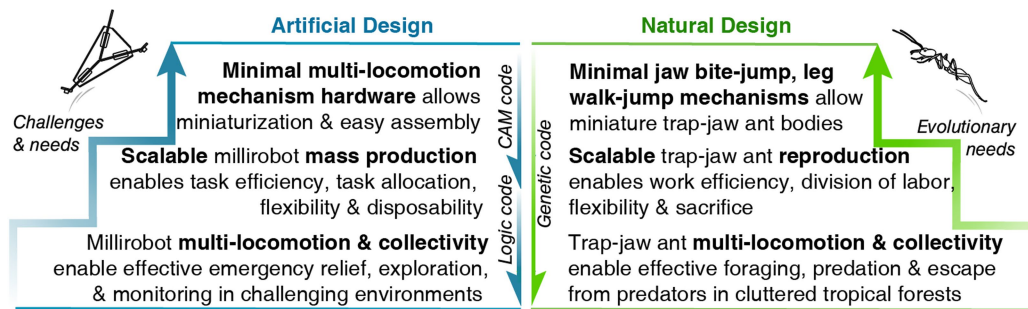
$$\gamma - \frac{\pi}{6} + m\pi \leq \beta_2 \leq \gamma + \frac{\pi}{6} + m\pi, \quad m = \dots -1, 0, 1, \dots \quad (16)$$

where  $\beta_1$  and  $\beta_2$  are the orientations of the first and the second robots on the ground  $x$ - $z$  Cartesian coordinate plane, respectively, and  $\gamma$  is the relative angle between the two robots.

## Data availability

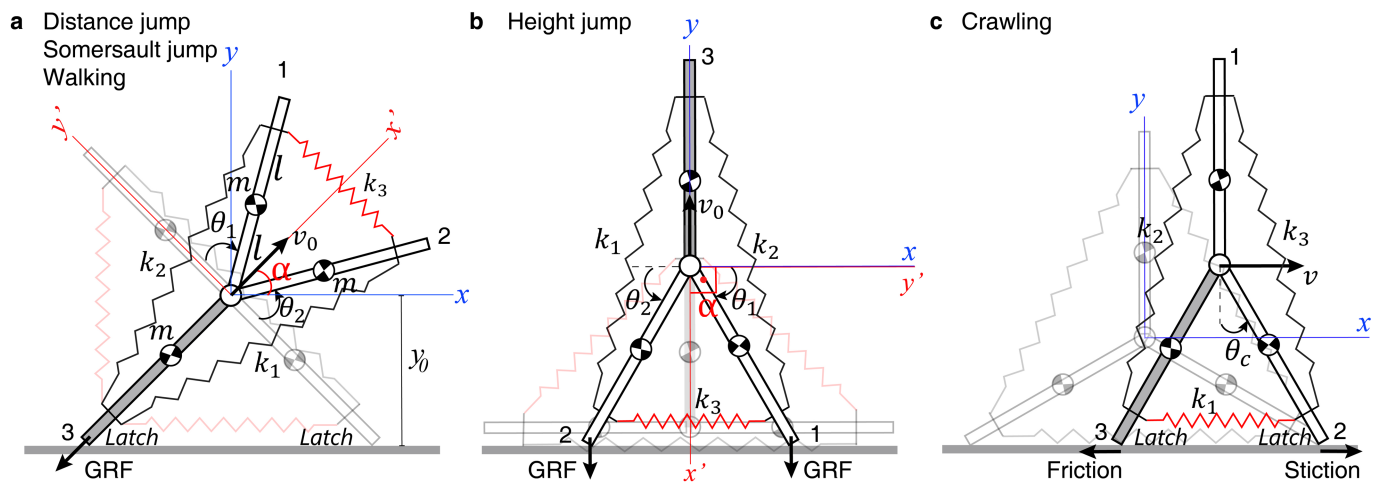
All data generated or analysed during this study are included in the published article, and are available from the corresponding author on reasonable request.





**Extended Data Fig. 1 | Design challenges and needs of biological versus artificial multi-locomotion collectives.** Trap-jaw ant collectivity, backed by scalable reproduction and the minimal multi-locomotion mechanisms that are integrated into their jaws and legs are the key to their survival in cluttered environments, which have emerged from evolutionary processes. Replicating these abilities in engineered systems will enable the use of millirobots in applications such as emergency mitigation,

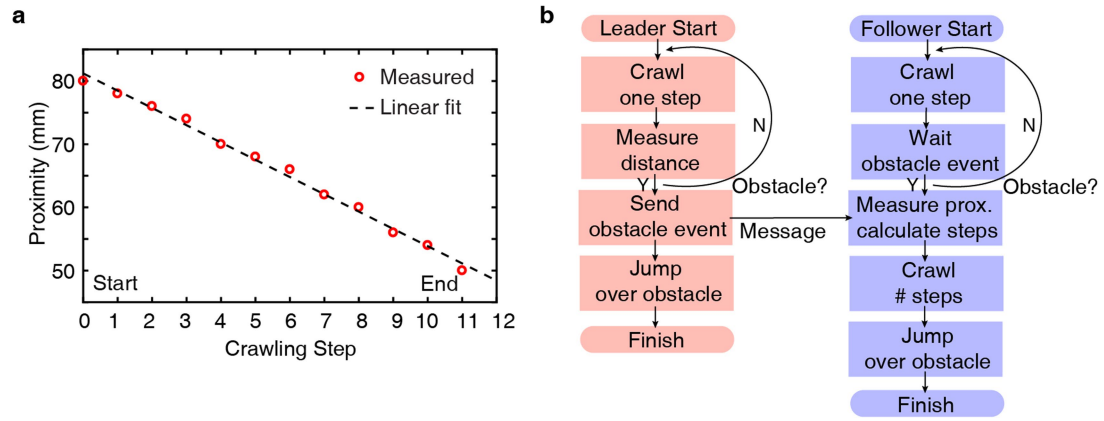
environmental monitoring and exploration with high task flexibility and efficiency. However, constructing minimal, integrated multi-locomotion mechanisms remains a major challenge for robotic hardware design that, when addressed, will enable robot miniaturization and assembly-free mass production for collective implementations. CAM, computer-aided manufacturing.



**Extended Data Fig. 2 | Free-body diagrams of Tribot for calculating the locomotion kinematics and dynamics for all five locomotion gaits.**

**a**, Tribot transitioning from initial stance to take-off, applicable for the distance- and somersault-jump gaits and walking gaits as a result of snap-through at the Y-hinge side. The Y-hinge is modelled as a revolute pin joint connecting three links. The snap-through motion generated by compression of the SMA spring actuator ( $k_3$ ) instantly rotates the side legs (1 and 2) and pushes the rear leg (3) against the ground. This produces a ground reaction force that lifts the robot in a ballistic projectile motion with take-off velocity  $v_0$ . For somersault jumping, the bottom spring

actuator ( $k_1$ ) activates shortly before the side spring ( $k_3$ ) to achieve free-body rotation during flight. **b**, The robot can perform height jumps on any three edges; however, for reaching high altitudes, it is most effective on the edge without rubber friction pads (which are located on legs 2 and 3). Here, the snap-through occurs at the Y-hinge bottom, and the rapid closing of the bottom legs produces a ground reaction force that lifts the robot up vertically. **c**, The crawling locomotion occurs on the edge with latches; the robot moves by opening and closing the bottom legs (2 and 3) using stick-slip motion. GRF, ground reaction force.



**Extended Data Fig. 3 | The proximity measurement data for the division-of-labour experiment and the event chart for the tandem-running experiment. a,** The proximity data measured by the monitor robot, showing the linear propagation of the workers with each pushing

step. The object is moved its set distance, 30 mm. **b,** The event chart for the leader–follower tandem-running experiment with obstacle avoidance by communication.



Extended Data Table 1 | Tribot's functional components and mass budget

Part/Layer	Material	Quantity	Mass (g)
Rigid legs	Fiberglass-Copper	1	3.1
Compliant hinge	Polyimide	1	0.49
SMA Actuators	Nitinol	5	0.35
Latch friction pads	Elastocil	4	0.5
Electronics & wires	Silicon, copper	>50	1.56
Batteries	Lithium-Polymer	3	3.7
<b>Robot Total</b>			<b>9.7</b>

Extended Data Table 2 | Tribot's locomotion performance under different conditions

	Experimental Condition	Mean Displacement (mm)	Standard Deviation (%)
1	Height jump, w/o latch	140.6	5
2	Height jump, w/ latch	72.5	7.5
3	Distance jump $P=3.7$ W	230	7.2
4	Distance jump $P=2.7$ W	140	8.8
5	Distance jump $P=3.7$ W, $L=5$ g	110	21.1
6	Somersault jump $P=3.7$ W	h: 88, d: 100	12.5
7	Walking on flat surface $P=1.7$ W	48.8	10.8
8	Walking on rough surface $P=1.7$ W	31.1	12.9
9	Walking onto slope $10^\circ$ , $P=2.2$ W	28.8	25.7
10	Crawling on flat surface	4.9	8
11	Crawling onto slope $10^\circ$	2.6	28.8

h, height; d, distance.

Extended Data Table 3 | Comparison of Tribot with small-scale terrestrial multi-locomotion robots and insects

Robot/Insect Name	Mass (g)	Size (mm)	Number of Locomotion	Energy Storage, Transmission & Actuation	Jump h./ Size	Jump d./ Size	COT (J.kg <sup>-1</sup> m <sup>-1</sup> )
JumpRoach [13]	59.4	100	2, crawling & jumping	6 rubber bands, 1 four-bar linkage leg, 3 gears, 3 DC motors	11.0	7.0	h: 9.7 d: 22.4
MSU Jump-Runner [14]	25	90	2, running & jumping	2 elastic strips, 1 slider-crank-cable leg, 8 gears, 2 DC motors	16.0	6.6	h: 9.8 d: 23.6
MiniWhegs [15]	146	90	2, running & jumping	1 steel spring, 2 four bar linkage legs, 2 chains, 2 DC motors, 4 Whegs	2.4	1.2	h: 10.5 d: 19.3
Surveillance Robot [16]	250	140	2, rolling & jumping	1 steel spring, 1 six-bar linkage leg, 4 gears, 3 DC motors, 2 wheels	2.9	2.9	h: 11.7 d: 11.7
Wheel-Hopper [17]	170	168	2, rolling & jumping	1 steel spring, 2 four-bar linkage legs, 4 gears, 3 DC motors, 2 wheels	0.7	0.3	h: 10.7 d: 23.7
Trap-Jaw Ant <i>Odontomachus bauri</i> [5]	0.01	13	3, jaw-jump, leg-jump, leg-walk	<i>Flexor-extensor jaw snap catapult &amp; leg muscles</i>	5.6 escape 2.4 defense	2.4 escape 17.2 defense	h: 0.4 d: 0.9 escape
Desert Locust <i>Schistocerca gregaria</i> [29]	3	60	3, leg-jump, leg-walk, flying	<i>Flexor-extensor leg muscle contraction</i>	9.8	10.0	h: 6.2 d: 6.1
Jump. Spider <i>Phidippus princeps</i> [30]	0.15	15	2, leg-jump, leg-walk	<i>Flexor-extensor leg muscle contraction</i>	0.3	4.0	h: 69.8 d: 5.7
<b>Tribot</b> (in this article)	<b>9.7</b>	<b>58</b>	<b>5, height jump, distance jump, somersault jump, walking &amp; crawling</b>	<b>3 SMA springs &amp; 2 SMA sheet, 3 tree linkage legs, 1 snap-bend Y-hinge, 2 rubber latches</b>	<b>2.4</b>	<b>4.0</b>	<b>h: 14.4 d: 4.5 s: 14.8 w: 4.4 c: &lt;1</b>

Data are from refs <sup>13-17</sup>. DC, direct current; h, height; d, distance; s, somersault; w, walking; c, crawling. Whег, wing-leg or wheel-leg.